Corrosion resistance of low SiC particle variation at low weight content on 1060 aluminum matrix composite in sulfate-contaminated seawater

Roland Tolulope Loto, Philip Babalola

PII: S2211-3797(19)30514-5
DOI: https://doi.org/10.1016/j.rinp.2019.102241
Article Number: 102241
Reference: RINP 102241

To appear in: *Results in Physics*

Received Date: 13 February 2019
Revised Date: 25 March 2019
Accepted Date: 25 March 2019

Please cite this article as: Loto, R.T., Babalola, P., Corrosion resistance of low SiC particle variation at low weight content on 1060 aluminum matrix composite in sulfate-contaminated seawater, *Results in Physics* (2019), doi: https://doi.org/10.1016/j.rinp.2019.102241

Corrosion resistance of low SiC particle variation at low weight content on 1060 aluminum matrix composite in sulfate-contaminated seawater

Roland Tolulope Loto[1*] and Philip Babalola[1]

[1]Department of Mechanical Engineering, Covenant University, Ota, Ogun State, Nigeria

*tolu.loto@gmail.com

+2348084283392

Abstract

The effect SiC particle sizes (3 µm, 9 µm 29 µm and 45 µm) at 2.5% weight content on the corrosion resistance of 1060 aluminum in sulfate and sulfate-chloride solution was studied by potentiodynamic polarization, open circuit potential measurement and optical microscopy. Results showed the presence of SiC increases the susceptibility of monolithic aluminum (0 µm SiC particle size) to corrosion. In the sulfate solution, the corrosion rate values increased from 0.074 mm/y to 0.556 mm/y at 3 µm SiC particle size after which a progressive decrease in corrosion rate was observed to 0.240 mm/y at 45 µm SiC particle size. The corrosion rate value in sulfate-chloride solution increased significantly with increase in SiC particle size from 0.580 mm/y (0 µm) to 1.181 mm/y at 45 µm. Open circuit potential plots show monolithic aluminum in both solutions is the most electronegative, though potential transients were quite visible on the plot from sulfate-chloride solution. The surface of the corroded 1060AlSiC specimens agree with the results from electrochemical test with extensive morphological damage.

Keywords: aluminum, silicon carbide, corrosion

Introduction

Monolithic aluminum alloys embedded with silicon carbide particulates have extensive structural applications cutting across aerospace, automobile, sports, electronics and power generation industries due to their higher specific strength, stiffness, wear, electrical and thermal conductivities, low coefficient of thermal expansion and wear resistance and relatively lower density compared to their ferrous counterparts [1-4]. The chemical stability of silicon carbide with aluminum results in strong bonding between the matrix and SiC particulates with limited

intermetallic phases. Research has focused on the mechanical and tribological behaviour of aluminum silicon matrix composites, weight fraction and heat treatment on the wear behavior of aluminum silicon matrix composites, characteristics of silicon carbide particles, aluminum matrix selection, and effect of preparation processes on the structure and performance of the composites [5-7]. However, it must be noted that ceramic particulates strongly influence the electrochemical, chemical and physical interaction of metal matrix composites with their environment of operation often leading to accelerated corrosion and microstructural deterioration of the matrix composites during service. These phenomena stem from galvanic reactions between the interacting microstructural species. Residual contaminants resulting from processing methods and the formation of intermetallic phases significantly influence the corrosion resistance of matrix composites. Hence, corrosion inhibits the performance of aluminum matrix composites leading to catastrophic failures, breakdown and plant shutdowns [8, 9]. Aluminium is known for its high resistance to corrosion, by automatically overlapping passive protective oxide film Al_2O_3, which prevents further oxidation. The presence of these phases in the structure can lead to a decrease in local corrosion resistance of alloy, which is related to the differences in electrochemical potentials, especially electrode potentials of the matrix and precipitate [10]. Extensive corrosion research on aluminum matrix composites have focused on the degradation effect of chlorides on the composites [11-13]. The microstructure and properties of SiC particle reinforced composites are affected by the particle size and volume fraction of the SiC particles [14-16]. This research focusses on the effect of low SiC weight content (2.5%) at limited SiC particle size variations on the corrosion resistance of monolithic 1060 aluminum in sulfate-chloride solution.

Experimental procedure

Materials and preparation

AA1060 aluminium metal (AA1060) was sourced from Aluminium Rolling Mills, Ota, Ogun State, Nigeria. Energy dispersive spectrometer analysis at Materials Characterization Laboratory, Department of Mechanical Engineering, Covenant University, Ota, Ogun State, Nigeria gave nominal (wt. %) composition shown in Table 1. Silicon carbide (SiC) particles at 3 μm, 9 μm, 29 μm and 45 μm particle size whose grit sizes are shown in Table 2 with nominal (wt. %) composition shown in Table 3 was purchased from Logitech, UK and added to AA1060 at equal

weight percentage of 7.5%. Stir casting technique was used to produce the aluminium silicon matrix composites (1060AlSiC). 5 kg of 1060 aluminium metal was liquefied after heating to 750 ºC in a 20Kg graphite crucible within a tilting furnace powered with diesel fuel. The temperature of the molten aluminium was determined with the aid of K-type thermocouple. Molten aluminium was subsequently discharged into mould preheated to 450 ºC. The melt was stirred with a mechanical stirrer made of galvanized Fe to give a fine vortex at 500 revolutions per minute. Silicon carbide particles (SiC) at 2.5 vol. wt % (preheated to 1100 ºC) were mix with the vortex at 500 rpm for approximately 5 min. The process was repeated for 1060AlSiC at particle sizes of 3 µm, 9 µm, 29 µm and 45 µm with the same weight percentage (2.5 wt. %). The 1060AlSiC specimens produced through the stir casting method are of cylindrical shape with diameter of 110 mm and height of 30 mm. The cast specimens were machined after cooling with emery papers (80, 320, 600, 800 and 1000 grit), cleansed with deionized water and propanone, and kept in a desiccator for mechanical, electrochemical test and corrosion potential measurement. Analar grade NaCl purchased from Qualikems, India was prepared in molar concentration of 0.3 M while H_2SO_4 acid (analar grade 98%) was prepared in molar concentration of 0.05 M H_2SO_4 with deionized water.

Potentiodynamic polarization test

Potentiodynamic polarization was performed on 1060AlSiC specimens with SiC particle sizes of 0 µm, 3 µm, 9 µm, 29 µm and 45 µm. Platinum is the counter electrode, Ag/AgCl the reference electrode and resin embedded 1060AlSiC is the working electrodes. The electrodes were placed within a glass container filled with 200 mL of 0.05 M H_2SO_4 and 0.05 M H_2SO_4+3.5% NaCl and connected to Digi-Ivy 2311 potentiostat. Polarization curves were produced at scan rate of 0.0015V/s from -1.2V and +0.75V. Corrosion rate, C_R (mm/y) was determined as shown below;

$$C_R = \frac{0.00327 \times C_d \times E_q}{D} \quad (1)$$

D is the density in (g/cm^3); E_q is the equivalent weight (g). 0.00327 is the corrosion rate constant.

Open circuit potential (OCP) measurement and optical microscopy characterization

OCP measurements were performed at step potential of 0.1V/s for 3600 s with Digi-Ivy potentiostat. Optical images of 1060AlSiC surface morphologies at 0 µm, 3 µm and 45 µm were captured and analysed with Omax trinocular metallurgical microscope.

Table 1 Chemical Composition (wt. %) of AA1060 aluminium Ingot

Element	Si	Fe	Cu	Mn	Mg	Cr	Ni	Zn	Ti	Ag
Composition (%)	0.086	0.281	<0.0002	<0.0005	0.0016	0.002	0.0023	0.0014	0.0097	<0.0001
Element	Be	Bi	Ca	Cd	Na	Sr	V	Zr	Co	Li
Composition (%)	0.0003	<0.0010	0.0007	0.0002	0.0002	0.0001	0.0079	0.0021	<0.0010	<0.0001
Element	B	P	Pb	Sn	Al					
Composition (%)	0.0004	<0.0010	<0.0005	<0.0010	99.6					

Table 2 Grit size of SiC particle sizes

Particle size (µm)	**Grit size**
3	1200
9	600
29	320
45	240

Table 3 Chemical Composition (wt. %) of SiC

Element	C	Al	Fe	Si	SiO2	Magnetic Iron	SiC
Composition (%)	0.5	0.3	0.2	0.8	0.6	0.04	97.6

Results and discussion

Potentiodynamic polarization studies

Potentiodynamic polarization plots of 1060AlSiC matrix composites at 0 µm, 3 µm, 9 µm, 29 µm and 45 µm SiC particle sizes in 0.05 M H_2SO_4 and 0.05 M H_2SO_4+3.5% NaCl solutions are shown in Figs. 1(a) and (b) while the results obtained from the polarizations test are shown in Table 4. Comparative observation of the corrosion rate values in both electrolyte solutions shows the presence of SO_4^{2-} ions in simulated seawater (3.5% NaCl) aggravates the corrosion rate of 1060AlSiC specimens compared to their corrosion rate values in 0.05 M H_2SO_4 solution. At 0 µm SiC particle size, the corrosion rate of 1060AlSiC is 0.074 mm/y (0.05 M H_2SO_4 solution) corresponding to a current density of 6.8 x 10^{-6} A/cm^2. The corrosion rate value increased to 0.556 mm/y at 3 µm SiC particle size before decreasing progressively to 0.240 mm/y at 45 µm SiC particle size. The relatively low corrosion rate value at 0 µm is due to the oxidation of monolithic Al resulting in the formation of corrosion resistant Al_2O_3 on the metal surface. SiC reinforcement at 3 µm particle size introduces inhomogeneities on the Al matrix surface. This enabled penetration of SO_4^{2-} ions due to discontinuity on the passive protective film thereby resulting in instantaneous increase in corrosion rate [17]. There is also the possibility that the 3 µm SiC reacts with the Al matrix in the presence of SO_4^{2-} leading to higher corrosion reactions

[18-20]. The progressive decrease in corrosion rate from 9 µm to 45 µm SiC particle size has been reported in previous research [21-22]. There is a strong possibility that increase in SiC particle size improves the interfacial bonding between the Al SiC particles, thus hindering diffusion of SO_4^{2-} ions. The relatively smaller size of Cl^- ions in 0.05 M H_2SO_4+3.5% NaCl is responsible for the higher corrosion rate reactions of 1060AlSiC matrix composite specimens in the electrolyte solution. The chlorides influenced the formation of soluble chlorinated aluminium hydroxide in the presence of oxygen, which also weakened protective oxide [8]. Cl^- ions diffuse through the protective films on 1060AlSiC, accelerating corrosion reactions while the combined electrochemical action of Cl^- and SO_4^{2-} ions are deleterious for the composites. Hence, the corrosion rate of 1060AlSiC increases with increase in Cl^- and SO_4^{2-} ions concentration. At 0 µm the corrosion rate of 1060AlSiC is 0.580 mm/y, this value increased to 1.181 mm/y at corrosion current density of 1.09 x 10^{-4} A/cm^2. The presence of Cl^- ions induces corrosion leading to rapid penetration at the end of discontinuities on the matrix composite. Crevice attack at the 1060AlSiC interfaces within the matrix results in the presence of galvanic cells which enhances the corrosion on the matrix.

The oxidation of 1060AlSiC surface in 0.05 M H_2SO_4 significantly involve competitive adsorption of SO_4^2 ions and O_2 leading to displacement of the major factor responsible for passivation of 1060AlSiC. This is evident in the anodic-cathodic shift of 1060AlSiC corrosion potential in 0.05 M H_2SO_4 solution. The anodic-cathodic Tafel slope values in this solution counterbalance each other compared to 0.05 M H_2SO_4+3.5% NaCl solution where the cathodic portaion of the Tafel slope has minimal significance. 1060AlSiC anodic shift (corrosion potential) in 0.05 M H_2SO_4+3.5% NaCl solution from 3 µm to 45 µm SiC particle size corroborates the earlier assertion on the combined deleterious action of Cl^- and SO_4^{2-} ions leading to greater surface deterioration of the matrix composite. The Tafel slope values show higher anodic activity for 1060AlSiC in the Cl^- + SO_4^{2-} electrolyte. This suggests that the adsorbed Cl^- and SO_4^{2-} ions strongly influence the mechanism of the corrosion reactions compared to SO_4^{2-} ion in 0.05 M H_2SO_4 solution. This assertion agrees with the higher corrosion rate results obtained in Cl^- and SO_4^{2-} anions solution. Observation of the polarization plots in Fig. 1(a) and (b) shows limited oxidation-reduction reactions before metastable pitting in the presence of Cl^-/SO_4^{2-} electrolyte [Fig. 1(a)] compared to SO_4^{2-} electrolyte. This is due to higher the

displacement reaction with adsorbed O_2 atoms on the matrix surface in Cl^-/SO_4^{2-} electrolyte. The lower anodic-cathodic slopes in Fig. 1(b) before metastable pitting activity supports the higher corrosion rates and anodic Tafel slope data.

Table 4 Potentiodynamic polarization data for 1060AlSiC (0 µm, 3 µm, 9 µm, 29 µm and 45 µm SiC particle sizes) in 0.05 M H_2SO_4 and 0.05 M H_2SO_4 + 3.5% NaCl solutions

0.05 M H_2SO_4							
SiC Particle Size (µm)	**Corrosion Rate (mm/y)**	**Corrosion Current (A)**	**Corrosion Current Density (A/cm^2)**	**Corrosion Potential (V)**	**Polarization Resistance, R_p (Ω)**	**Cathodic Tafel Slope, B_c (V/dec)**	**Anodic Tafel Slope, B_a (V/dec)**
0	0.074	6.80E-06	6.80E-06	-0.788	3780.00	-6.348	5.957
3	0.556	5.12E-05	5.12E-05	-0.839	501.50	-7.639	4.746
9	0.305	2.81E-05	2.81E-05	-0.820	913.20	-6.846	5.638
29	0.248	2.29E-05	2.29E-05	-0.919	1124.00	-6.143	5.362
45	0.240	2.22E-05	2.22E-05	-0.737	1160.00	-6.588	7.030
0.05 M H_2SO_4/3.5% NaCl							
SiC Particle Size (µm)	**Corrosion Rate (mm/y)**	**Corrosion Current (A)**	**Corrosion Current Density (A/cm^2)**	**Corrosion Potential (V)**	**Polarization Resistance, R_p (Ω)**	**Cathodic Tafel Slope, B_c (V/dec)**	**Anodic Tafel Slope, B_a (V/dec)**
0	0.580	5.34E-05	5.34E-05	-1.042	480.80	-1.801	12.690
3	0.892	8.22E-05	8.22E-05	-0.682	312.40	-4.231	23.810
9	0.984	9.07E-05	9.07E-05	-0.722	272.00	-2.198	24.680
29	1.072	9.88E-05	9.88E-05	-0.733	221.90	-2.976	22.820
45	1.181	1.09E-04	1.09E-04	-0.795	173.60	-4.823	15.330

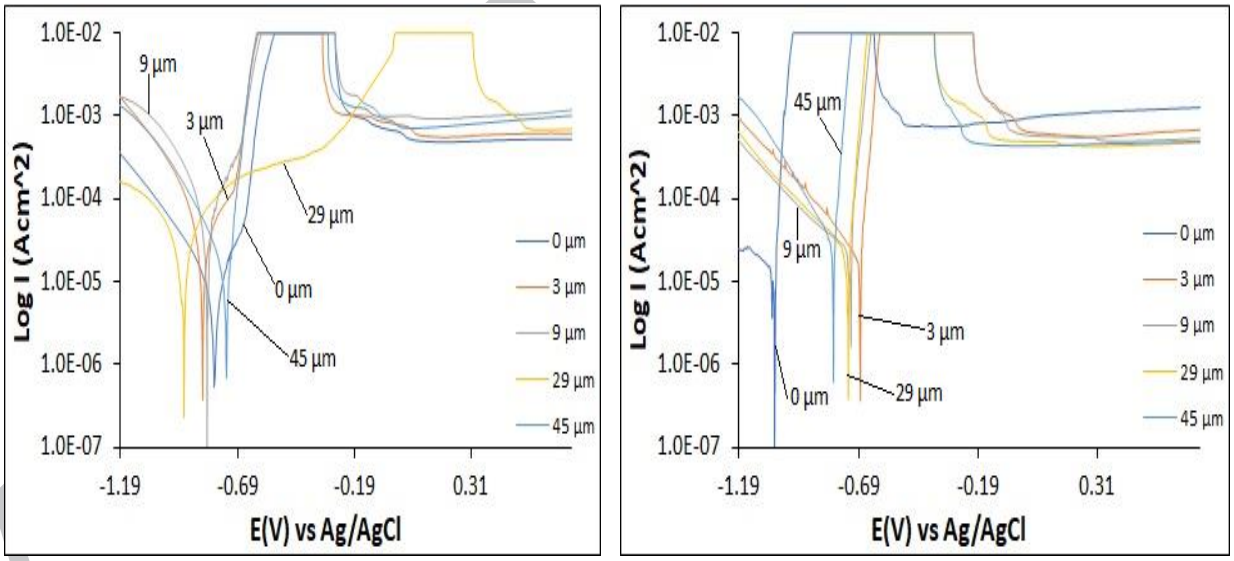

(a) (b)

Fig. 1 Potentiodynamic polarization plot for 1060AlSiC (0 µm, 3 µm, 9 µm, 29 µm and 45 µm SiC particle sizes) in 0.05 M H_2SO_4 and 0.05 M H_2SO_4 + 3.5% NaCl solutions

Open circuit potential analysis (OCP)

The OCP plots for 1060AlSiC in 0.05 M H_2SO_4 and 0.05 M H_2SO_4 + 3.5% NaCl solution at 0 µm, 3 µm and 45 µm SiC particle sizes are shown in Figs. 2(a) and (b). Figs. 3(a) – (c) and Figs. 4(a) – (c) shows the surface morphologies (mag. x40) of 1060AlSiC at 0 µm, 3 µm and 45 µm SiC particle sizes after OCP test. The OCP plots of 1060AlSiC at 0 µm SiC particle size in both electrolytes were generally more electronegative than the plots at 3 µm and 45 µm SiC particle size. In 0.05 M H_2SO_4 solution, 1060AlSiC plot (0 µm SiC particle size) decreased sharply from -0.782 $V_{Ag/AgCl}$ at 47.6 s to -1.086 $V_{Ag/AgCl}$ (1298.81 s) after which it remained generally stable till -1.093 $V_{Ag/AgCl}$ at 2237.62 s. The decrease in OCP value is due to breakdown of the protective film on the Al alloy surface leading to anodic dissolution of the Al substrate. The morphology in Fig. 3(a) shows the presence of corrosion pits which serves as the sites for breakdown of the passive film. Beyond 2237.62 s, a progressive increase in corrosion potential occurred up to -0.964 $V_{Ag/AgCl}$ due to repassivation of the protective film. The subsequent progressive increase is attributed to the gradual response of aluminum alloy constituents to SO_4^{2-} ions. Similar phenomenon was observed for the OCP plot at 3 µm SiC particle size (0.05 M H_2SO_4 solution). However, the associated morphology [Fig. 3(b)] shows superficial deterioration along the grain boundary. OCP plot of 1060AlSiC at 45 µm SiC particle size was relatively more electropositive than the two previous plots. The plot also depicts thermodynamic instability throughout the exposure period probably resulting from galvanic effects between the monolithic aluminum substrate and the 45 µm SiC particles as shown in the heterogeneous surface in Fig. 3(c). The electropositive plot may not be as a result of the growth of thicker Al_2O_3 oxide on the matrix surface. The larger SiC particle size possibly influences the corrosion resistance of the matrix alloy despite the discontinuities on the protective film on the matrix.

The OCP plot in Fig. 2(a) is strongly influenced by the presence of Cl^- ions in the sulfate/chloride solution as shown in the visible potential transients. The transients are the result of the formation of soluble chlorinated aluminum hydroxide which limits the stability of the oxide on the aluminum surface [23]. 1060AlSiC plot at 0 µm SiC particle size is the most electronegative throughout with intergranular corrosion in addition to pitting appearing on its morphology as shown in Fig. 4(a). Between 0 s and 321 s, the OCP plot decreased drastically to -1.1284 $V_{Ag/AgCl}$ due to gradual formation of the oxide film as earlier mentioned. At 488 s, a

progressive increase in corrosion potential was observed to -0.869 at 1228.22 as a result of the formation of the protective film after which the OCP plot remained generally stable till 3600 s. The potential transients result from the electrochemical action of chlorides resulting in the rupture and subsequent reformation of the protective film [24]. In reality the film is practically unstable. The extent of variation of the potential transients on the OCP plots of 1060AlSiC at 3 µm and 45 µm SiC particle sizes is much lower coupled with a relatively stable OCP plot with respect to time due to the presence of SiC in the aluminum substrate. In Fig. 4(b), intergranular corrosion is prevalent at specific sites on the surface. Though the extent of intergranualr damage is much higher, the associated OCP plot shows the protective oxide film reformed. No remarkable damage is visible on Fig. 4(c) apart from some specific deterioration. The protective film on 1060AlSiC generally provides sufficient protection under appropriate conditions. However, in the presence of Cl^-, rupture of the oxide film occurs at specific sites leading to deterioration on the aluminum matrix surface [25].

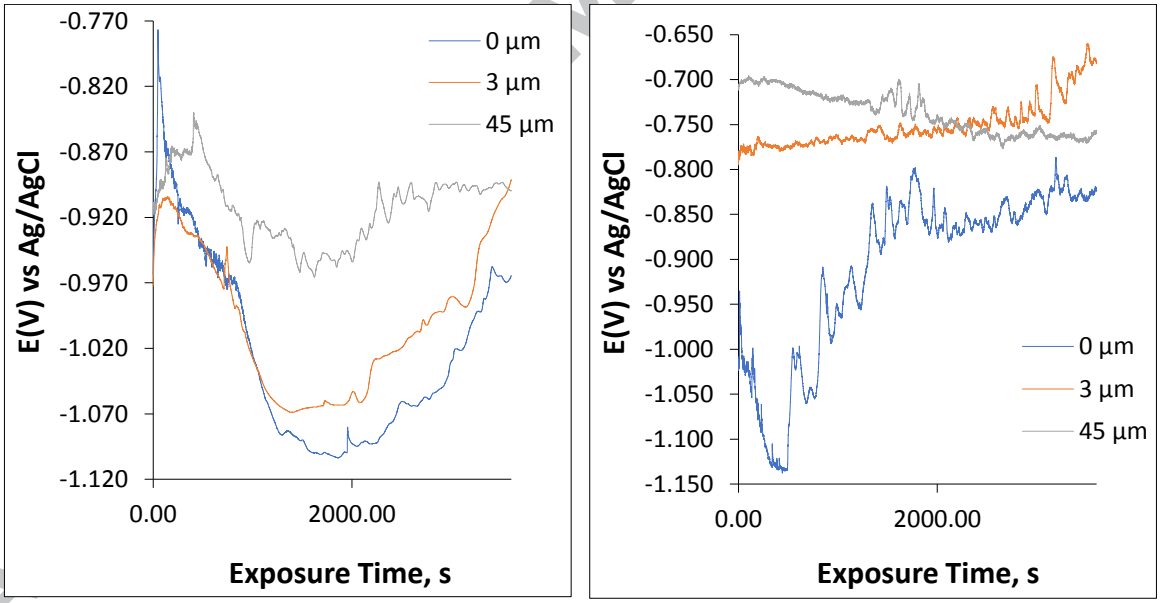

(a) (b)

Fig. 2 Open circuit potential measurement of 1060AlSiC at 0 µm, 3 µm and 45 µm SiC particle sizes in (a) 0.05 M H_2SO_4 and (b) 0.05 M H_2SO_4 + 3.5% NaCl solutions

(a) (b) (c)

Fig. 3(a) Optical morphology of 1060AlSiC from OCP test in 0.05 M H_2SO_4 solution at (a) 0 µm, (b) 3 µm and (c) 45 µm SiC particle sizes

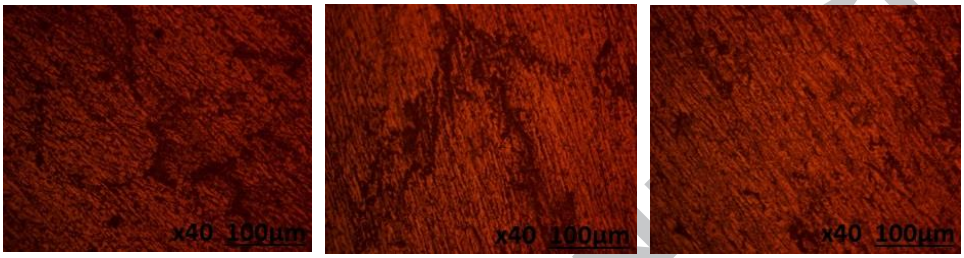

(a) (b) (c)

Fig. 4(a) Optical morphology of 1060AlSiC from OCP test in 0.05 M H_2SO_4 + 3.5% NaCl solution at (a) 0 µm, (b) 3 µm and (c) 45 µm SiC particle sizes

Optical microscopy characterization

Fig. 5(a) – (c) shows the optical microscopy images of 1060AlSiC (0 µm, 3 µm and 45 µm SiC particle size) morphology before corrosion while Fig. 6(a) – 7(c) shows the optical images of 1060AlSiC after corrosion in 0.05 M H_2SO_4 and 0.05 M H_2SO_4 + 3.5% NaCl solution. Fig. 5(a) and (b) are generally similar in morphology, whereas the 45 µm SiC particle size on the morphology of 1060AlSiC [Fig. 5(c)] giving it a coarse like appearance. The optical images of 1060AlSiC in Fig. 6(a) – (c) reflect the results from the potentiodynamic test. Limited surface deterioration occurred on 1060AlSiC at 0 µm SiC particle size in the presence of SO_4^{2-} ions. At 3 µm SiC [Fig. 6(b)] particle size the extent of general surface deterioration has increased due to galvanic effects resulting from the presence of SiC particles. The deterioration appears to be region specific indicating sits where discontinuities in the protective film leading to intiatial of interfacial corrosion reactions. Fig. 6(c) shows that increase in SiC particle size to 45 µm increases the resistance of 1060AlSiC to surface deterioration though the extent of deterioration is much higher than shown in Fig. 6(a). Addition of 3.5% NaCl solution to the sulfate media increases the degree of surface deterioration of 1060AlSiC at specific SiC particle size. However, potentiodynamic polarization results shows increase in SiC partcle sizes cause a

propotionate increase in corrosion rate of 1060AlSiC. The morphology of 1060AlSiC from from Fig. 7(a) – (c) confirms the electrochemical test results as the extent of morphological damages varies with SiC particle size. Observation of Fig. 7(a) shows wide ranging deterioration, however Fig. 7(b) and (c) SiC particle size increase does not necessarily increase the coverage of deterioration but instead concentrates at specific sites on 1060AlSiC surface. This observation is due to the electrochemical action of chlorides whose effect tends to be specific as a result of their ability to diffuse through breakages and weak points on the protective film.

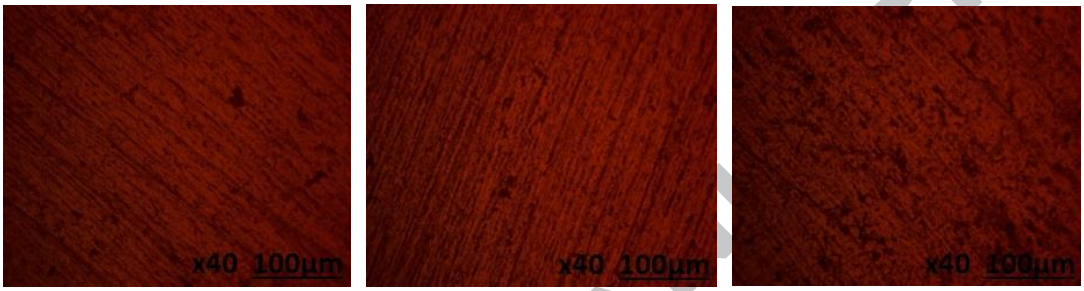

(a) (b) (c)

Fig. 5 Optical images of 1060AlSiC before corrosion (a) 0 µm, (b) 3 µm and (c) 45 µm SiC particle sizes

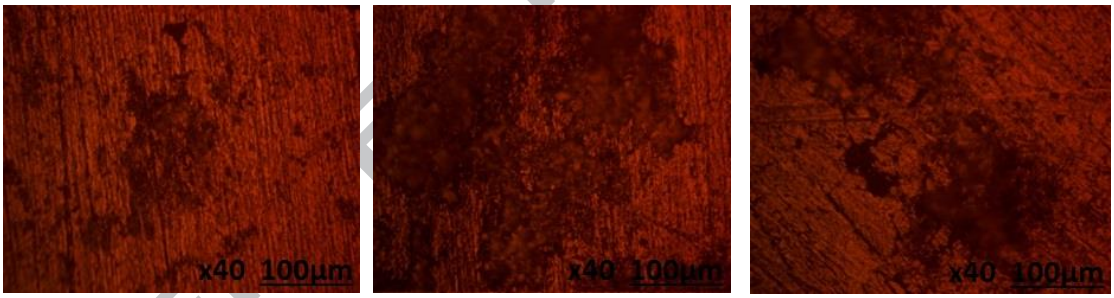

(a) (b) (c)

Fig. 6 Optical images of 1060AlSiC after corrosion in 0.05 M H_2SO_4 solution (a) 0 µm, (b) 3 µm and (c) 45 µm SiC particle sizes

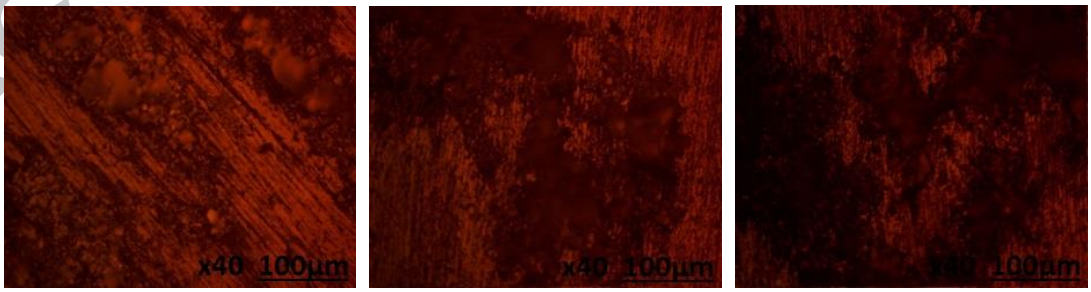

(a) (b) (c)

Fig. 7 Optical images of 1060AlSiC after corrosion in 0.05 M H_2SO_4 + 3.5% NaCl solution (a) 0 µm, (b) 3 µm and (c) 45 µm SiC particle sizes

Conclusion

Variation of SiC particle sizes at low SiC content strongly influences the corrosion resistance of 1060 aluminum matrix composites in sulfate and chloride-sulfate solution. In sulfate, higher SiC particle size results in decrease in corrosion rate while significant increase in corrosion rate occurred in sulfate-chloride solution. At rest potentials (no applied potential) higher SiC particle size reduces the thermodynamic tendency of 1060AlSiC to corrode. Optical microscopy shows morphological deterioration of 1060AlSiC is proportional to the type and concentration of corrosive anions present.

Acknowledgement

The author of the publication is grateful to Covenant University, Ota, Ogun State, Nigeria for their support provision of research facilities.

References

1. Hassan, A.M., Abdalla Alrashdan, A.T.M., Hayajneh, M.T. (2008) Wear behavior of Al–Cu and Al–Cu/SiC components produced by powder metallurgy, *Journal of Material Science*, 43, 5368-5375.
2. Chawla, N., Chawla, K.K. (2006) Metal Matrix Composites, Springer Science, Business Media, Inc.
3. Dsa, D.K., Mishra, P.C., Singh, S. (2014) Properties of ceramic-reinforced aluminium matrix composites-a review, *International Journal of Mechanical and Materials Engineering*, 9, 12-18.
4. Mazahery, A., Shabani, M.O. (2013) Application of the extrusion to increase the binding between the ceramic particles and the metal matrix: Enhancement of mechanical and tribological properties, *Journal of Materials Science and Technology*, 2013, 29, 423-428.
5. Liu, Z.S., Huang, B., Mingyuan Gu, M. (2006) Corrosion behavior of Al/AlNp composite in alkaline solution, *Materials Letters*, 60, 2024-2028.
6. Durai, T.G., Das, K., Siddhartha Das, S. (2007) Effect of mechanical milling on the corrosion behavior of Al–Zn/Al2O3 composite in NaCl solution, *Journal of Materials Science*, 42, 8209-8214.

7. Saber, K.A.D., Sallam, H.E.M. (2015) Wear and corrosion behavior of Al–Si matrix composite reinforced with alumina, *Journal of Bio- and Tribo-Corrosion*, 1, 5. https://doi.org/10.1007/s40735-014-0005-5
8. Loto, R.T., Babalola, P. (2017) Corrosion polarization behavior and microstructural analysis of AA1070 aluminium silicon carbide matrix composites in acid chloride concentrations, *Cogent Engineering*, 4, 1422229. https://doi.org/10.1080/23311916.2017.1422229.
9. Loto, R.T., Babalola, P. (2018) Effect of alumina nano-particle size and weight content on the corrosion resistance of AA1070 aluminum in chloride/sulphate solution, *Results in Physics*, 10, 731–737.
10. Kwiatkowski, L. (2009) Susceptibility to corrosion and effectiveness of actual methods of corrosion protection of aluminum alloys applied in civil engineering, *Surface Engineering*, 4, 24-33.
11. Kiourtsidis, G., Skolianos, S.M. (2007) Pitting corrosion of artificially aged T6 AA2024/SiCp composites in 3.5 wt.% NaCl aqueous solution, *Corrosion Science*, 49, 2711-2725.
12. Gopinath, K., Balasubramaniam, R., Murthy, V.S.R. (2001) Corrosion behavior of cast Al–Al_2O_3 particulate composites, *Journal of Materials Science Letters*, 20, 793-794.
13. De Salazar, J.M.G., Urena, A., Manzanedo, S., Barrena, M.I. (1999) Corrosion behaviour of AA6061 and AA7005 reinforced with Al_2O_3 particles in aerated 3.5% chloride solutions: potentiodynamic measurements and microstructure evaluation. Corrosion Science, 41, 529-545.
14. Alaneme, K.K., Adewale, T.M., Olubambi, P.A. (2008) Corrosion and wear behaviour of Al-Mg-Si alloy matrix hybrid composites reinforced with rice husk ash and silicon carbide, *Journal of Materials Research and Technology*, 3, 9-16.
15. Valdez, S., Campill, B., Perez, R., Martine, L., Garcia, A. (2008) Synthesis and microstructural characterization of Al-Mg alloy-SiC particle composite, *Materials Letters*, 62, 2623-2625.
16. Loto, R.T., Babalola, P. (2018) Analysis of SiC grain size variation and NaCl concentration on the corrosion susceptibility of AA1070 aluminium matrix composites, *Cogent Engineering*, 5, 1473002. https://doi.org/10.1080/23311916.2018.1473002.

17. Trowsdale, A.J., Noble, B., Harris, S.J., Gibbins, I.S.R., Thompson, G.E., Wood, G.C. (1996) The influence of silicon carbide reinforcement on the pitting behaviour of aluminium, *Corrosion Science*, 38(2), 177–191.
18. ASM Handbook. Composites, 2001;21.
19. ASM Handbook. Corrosion, 4th ed., 1992;13.
20. Paciej, R.C., Agarwala, V.S. (1986) Metallurgical variables influencing the corrosion susceptibility of a powder metallurgy aluminum/SiCw composite, *Corrosion*, 42(12), 718-729.
21. Feng, Z., Lin, C., Lin, J., Luo, J. (1998) Pitting behavior of SiC /2024 Al metal matrix composites, *Journal of Material Science*, 33, 5637-5642.
22. Candan, S. (2004) Effect of SiC particle size on corrosion behavior of pressure infiltrated Al matrix composites in a NaCl solution, *Materials Letters*, 58, 3601-3605.
23. Sukiman, N.L., Zhou, X., Birbilis, N., Hughes, A.E., Mol, J.M.C., Garcia, S.J., Zhou, X., Thompson, G.E. (2012) Durability and corrosion of aluminum and its alloys: overview, property space, techniques and developments, in: Aluminum Alloys—New Trends in Fabrication and Applications ed. by Ahmad Z, InTech, Rijeka.
24. Loto, R.T., Adeleke, A. (2016) Corrosion of aluminum alloy metal matrix composites in neutral chloride solutions, *Journal of Failure Analysis and Prevention*, 16(5), 874–885.
25. Ezuber, H., El-houd, A., El-shawesh, F. (2008) A study on the corrosion behavior of aluminum alloys in seawater, *Materials Design*, 29(4), 801–805.

- Effect SiC particle sizes on the corrosion resistance of 1060 Al in sulfate-chloride solution was studied
- SiC increases the susceptibility of monolithic aluminum (0 μm SiC particle size) to corrosion
- Corrosion rate decreased with increase in SiC particle size at low weight content in sulphate solution
- Corrosion rate increased with increase in SiC particle size in chloride/sulphate solution
- Open circuit potential plots show monolithic aluminum in both solutions is the most electronegative